THE JOURNAL OF PHYSICAL CHEMISTRY A

ARTICLE

pubs.acs.org/JPCA

Electronic Absorption Spectra of Protonated Pyrene and Coronene in Neon Matrixes

Iryna Garkusha,[†] Jan Fulara,[†,‡] Peter J. Sarre,[§] and John P. Maier*[,†]

[†]Department of Chemistry, University of Basel, Klingelbergstrasse 80, CH-4056 Basel, Switzerland

[‡]Institute of Physics, Polish Academy of Sciences, Al. Lotników 32/46, PL-02668 Warsaw, Poland

[§]School of Chemistry, University of Nottingham, University Park, Nottingham NG7 2RD, United Kingdom

ABSTRACT: Protonated pyrene and coronene have been isolated in 6 K neon matrixes. The cations were produced in the reaction of the parent aromatics with protonated ethanol in a hot-cathode discharge source, mass selected, and co-deposited with neon. Three electronic transitions of the most stable isomer of protonated pyrene and four of protonated coronene were recorded. The strongest, $S_1 \leftarrow S_0$ transitions, are in the visible region, with onset at 487.5 nm for protonated pyrene and 695.6 nm for protonated coronene. The corresponding neutrals were also observed. The absorptions were assigned on the basis of ab initio coupled-cluster and time-dependent density functional theory calculations. The astrophysical relevance of protonated polycyclic aromatic hydrocarbons is discussed.

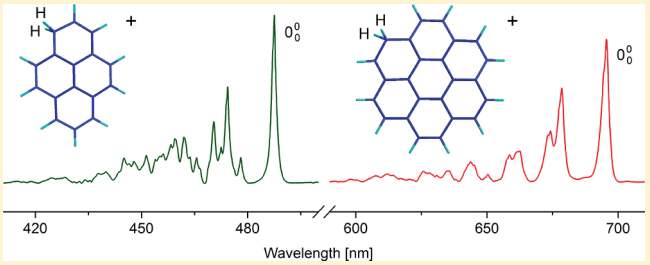

1. INTRODUCTION

The astrophysical significance of polycyclic aromatic hydrocarbons (PAHs) has been discussed in the literature.[1] Recently, protonated PAHs (H-PAH$^+$s) became the topic of both quantum chemical and experimental interest because of their role as possible carriers of unidentified infrared emission bands (UIRs)[2] and diffuse interstellar bands (DIBs).[3−5] A number of H-PAH$^+$s have been studied in the gas phase using single-photon IR photodissociation spectroscopy and the messenger-atom method[6−8] or by IR multiphoton dissociation using free-electron lasers.[9−11] The largest molecule studied so far is protonated coronene, whose IR spectrum resembles astronomical UIR features to some extent.[11]

Electronic transitions of a number of protonated PAHs have been studied in strong acidic solutions;[12−16] however, these transitions are strongly perturbed by the liquid environment. Recently, electronic spectra of medium-sized H-PAH$^+$s in neon matrixes[17,18] and in the gas phase obtained using laser photofragment spectroscopy[19,20] have been reported.

In this contribution, electronic absorption spectra of larger H-PAH$^+$s, namely, protonated pyrene (H-Py$^+$) and protonated coronene (H-Cor$^+$), and their neutral radical counterparts, H-Py and H-Cor, isolated in 6 K neon matrixes are reported. These studies provide wavelengths and relative intensities of the bands of these species that can be used as a starting point for gas-phase measurements and for evaluating their astrophysical relevance.

2. EXPERIMENTAL SECTION

2.1. Matrix Isolation. Electronic spectra of protonated pyrene and coronene cations were recorded using ion-beam mass selection and the matrix isolation technique. The apparatus used was described previously.[21] H-Py$^+$ and H-Cor$^+$ were generated in a hot-cathode discharge source in a reaction of PAH vapor with protonated ethanol (H-Eth$^+$) (section 2.2). Cations were extracted from the source using electrostatic lenses and guided through a static bender, where they were separated from neutral molecules, and then into a quadrupole filter. After mass selection, the cations of interest were deposited with a 20000:1 mixture of neon and CH_3Cl onto a rhodium-coated sapphire plate cooled with a closed-cycle He cryostat to 6 K. The CH_3Cl was used as an electron scavenger; it suppresses ion neutralization during deposition by capturing free electrons and reduces the space charge in the matrix. The neon layer was grown to ∼150-μm thickness, which was monitored by observing the light transmittance through the matrix.

The spectra were recorded in the range 220−1100 nm in a "wave-guide" manner by passing broadband light from a halogen or high-pressure Xe arc lamp through the matrix. A bundle of 50 optical fibers transmitted the light, which had passed through the 20-mm-long neon matrix, to the entrance slit of a 0.3-m spectrograph. It was equipped with three rotatable gratings dispersing the light onto an open-electrode or a back-illuminated CCD camera.

Pyrene and coronene samples were resistively heated to get an appropriate vapor pressure. The ion current achieved for H-PAH$^+$s was in the range 5−20 nA and resulted in a total accumulated charge of ∼42 μC for H-Py$^+$ and ∼60 μC for H-Cor$^+$.

2.2. Production of Ions. Protonated PAHs previously studied in this laboratory (protonated benzene,[17] anthracene and

Received: June 30, 2011
Revised: August 21, 2011
Published: August 23, 2011

dx.doi.org/10.1021/jp206188a | J. Phys. Chem. A 2011, 115, 10972–10978

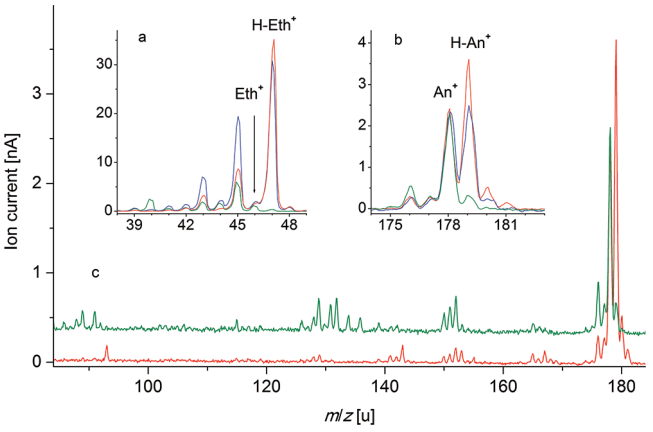

Figure 1. Mass spectra of ions produced in the reaction of anthracene with protonated ethanol in a hot-cathode discharge source at different pressures of ethanol: green trace—low; blue—intermediate conditions; red—highest ethanol pressure, optimized for maximum intensity of protonated anthracene. Insets show increase of (a) protonated ethanol and (b) protonated anthracene with increasing ethanol pressure, whereas (c) displays the influence of ethanol on the fragmentation of anthracene. All spectra are normalized to the same intensity of An^+.

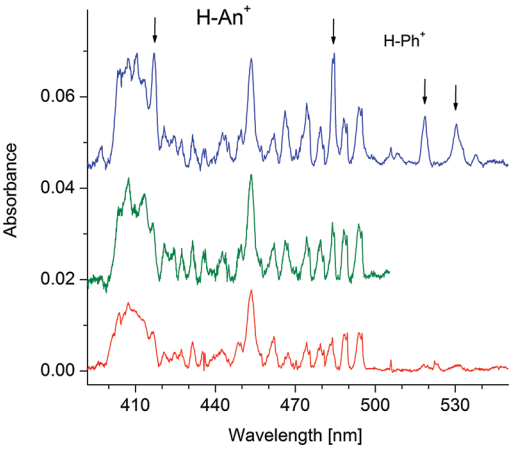

Figure 2. Electronic spectrum of $C_{14}H_{11}^+$ produced in the reaction of anthracene with protonated ethanol (bottom trace) compared to that observed when 9,10-dihydroanthracene used as a precursor (top trace). The absorption bands of protonated phenanthrene (indicated by arrows) are present in the latter case as a result of isomerization in the source. The middle trace is the "clean" spectrum of protonated anthracene after correction for the absorptions of protonated phenanthrene.

phenanthrene[18]) were produced from the respective dihydro-PAHs in a hot-cathode discharge ion source. The H-PAH$^+$ cations were formed through ionization of the parent neutral and removal of a H atom from one of the CH_2 groups. Fragmentation and isomerization of ions were observed in such experiments and complicated the interpretation of the spectra.[18] H_2-Py and H_2-Cor were, however, not available; therefore, another production method was needed.

Chemical ionization and proton transfer are energetically milder ionization methods,[22] frequently used in mass-spectrometric studies. PAHs have relatively high proton affinities (PAs);[23] therefore, their protonated analogues can be generated in proton-transfer reactions. This has been achieved in an ion cyclotron resonance mass spectrometer for small PAHs and some heterocyclic aromatics using CH_5^+ or $C_2H_5^+$ as the proton donor.[8,24] A similar method was applied in the present work for the generation of protonated PAHs. The electronic spectrum of protonated anthracene (H-An$^+$) is known from our previous work,[18] where 9,10-dihydroanthracene was used as a precursor. Assignment of the carrier of the absorption bands was complicated by the presence of a number of m/z = 179 isomers in the matrix. Therefore, to evaluate and compare the proton-transfer approach to the formation of larger H-PAH$^+$s with the method used earlier,[18] a number of experiments were undertaken in the course of this study using anthracene (An).

In the reaction of An with H_3^+ or CH_5^+, no protonation of the PAH was observed, and only parent An^+ signals were present in the mass spectrum. Although the PAs of H_2 (424 kJ/mol) and CH_4 (536 kJ/mol)[23] are much lower than that of An, so that proton donation is energetically feasible, the excess energy in the reaction appears to be too high to be dissipated through internal vibrational relaxation, and the formation of PAH$^+$ is favored. H-Eth$^+$ was chosen as the next proton donor because the PA of C_2H_5OH (776 kJ/mol) is higher than those of the reagents above, but still lower than that of An.

Mass spectra of the anthracene/ethanol system obtained using different conditions in the ion source are shown in Figure 1. At a low source pressure of ethanol, both substances are ionized by electrons (Figure 1, green trace). The mass spectrum is characterized by the parent cation (m/z = 178) of An (Figure 1b) and, in the low-mass range, by the fragment of ethanol with m/z = 45 (Figure 1a), which is in agreement with the data obtained using electron ionization.[25] At higher pressures in the source, H-Eth$^+$ is formed, and the simultaneous growth of the m/z = 179 cation, H-An$^+$, is observed (Figure 1, blue line). A further increase of the pressure results in more efficient production of both protonated species (Figure 1, red trace). An^+ ions are still present (Figure 2b, where the spectra are normalized to the same intensity of An^+), but the high intensity of H-An$^+$ indicates the efficiency of protonation.

The electronic spectrum of the m/z = 179 cations produced in the reaction described above was measured (Figure 2, lower trace) and compared with that observed when dihydroanthracene was used as a precursor (Figure 2, upper trace). As discussed,[18] the latter contains not only the absorptions of H-An$^+$, but also the bands of protonated phenanthrene (H-Ph$^+$), which are present as a result of isomerization in the ion source. The spectrum corrected for these absorptions, shown as middle trace of Figure 2, closely resembles the lower one, obtained in the reaction of An with H-Eth$^+$, showing only the H-An$^+$ features.

Thus, the relatively small difference in the PAs of ethanol and anthracene reduces the isomerization of the cations in the source (Figure 2); furthermore, it ensures generation of H-An$^+$ with less fragmentation of the precursor (Figure 1c). Therefore, this method was used for the production of H-Py$^+$ and H-Cor$^+$. As the PAs of Py and Cor are similar to that of An, H-Eth$^+$ was chosen as the protonation reactant.

3. RESULTS AND DISCUSSION

3.1. Protonated Pyrene. The recorded electronic spectrum of m/z = 203 cations produced in the reaction of Py with H-Eth$^+$ and deposited in a neon matrix is dominated by two absorption features located at 487 and 389 nm (Figure 3, blue line). Aside

dx.doi.org/10.1021/jp206188a |J. Phys. Chem. A 2011, 115, 10972–10978

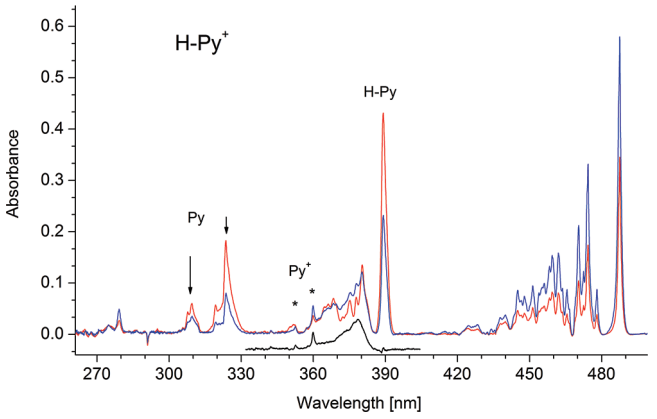

Figure 3. Absorption spectra recorded after deposition of $C_{16}H_{11}^+$ into a neon matrix (blue) and after photobleaching with UV photons (red). Weak bands of neutral pyrene and its radical cation are indicated by arrows and asterisks, respectively. The black trace shows weak absorption of protonated pyrene, obtained after scaling the red trace to the intensity of the absorption at 389 nm and subtracting it from the blue trace.

from these, the strongest known bands of Py^+ and Py are weakly seen in the spectrum at 360 and 323 nm, respectively.[26,27] There are two reasons for Py^+ absorptions being observed. First, ^{13}C isotopologues of Py^+, which have the same m/z ratio as H-Py^+, are deposited together with the ions of interest. In addition, fragmentation of H-Py^+ can take place. The absorptions of Py^+ are weak in the present experiment, indicating almost complete protonation of Py in the source. Bands of Py are the result of partial neutralization of Py^+ and/or fragmentation of H-Py^+ upon deposition.

After irradiation of the matrix with a medium-pressure Hg lamp, the 487-nm system decreased, and the other at 389 nm gained intensity (Figure 3, red line). The known bands of Py^+ behave in the same manner—they decrease in intensity after irradiation and give rise to the absorptions of Py. No new bands appeared in the spectrum. Upon irradiation, the trapped cations are neutralized by electrons, which are released from an electron scavenger present in the matrix. These are Cl^- anions, formed when CH_3Cl molecules capture electrons released during deposition.[21] Thus, the 487-nm system is due to H-Py^+ and that at 389 nm belongs to the corresponding neutral H-Py radical. The two systems are characterized by strong, sharp origin bands followed by similar, complex vibrational structures showing excitations in the same vibrational fundamentals. For instance, the 570/591 and 747/762 cm^{-1} modes are active in the excited states of H-Py^+ and its neutral, respectively. Wavelengths of the maxima of the observed bands are given in Table 1.

Two other bands of cationic origin are also assigned to H-Py^+. The first is a weak system originating at 279 nm (Figure 3). The second is a band hidden by the strong 389-nm absorption of H-Py. It is seen better when the spectrum recorded after irradiation is subtracted from that recorded after deposition, scaled to the intensity of the strong 389-nm peak. It is the broad band centered at 378 nm (Figure 3, black trace). In the past, H-Py^+ has been studied in strong acidic solutions[14,15] and in H^+-zeolites.[28] Two broad electronic absorption bands of H-Py^+ were observed at around 475 and 380 nm. The wavelengths of these absorptions are close to those observed presently.

Table 1. Absorption Band Maxima (±0.1 nm) Observed for the Electronic Transitions of Protonated Pyrene[a] and the Corresponding Neutral in a Neon Matrix, and Calculated Vertical Excitation Energies ΔE

λ (nm)	ΔE^b (eV)	$\tilde{\nu}$ (cm^{-1})	$\Delta\tilde{\nu}$ (cm^{-1})		assignment[c]
1H-Py$^+$					
487.5 (1)	**2.80**/*2.61*	20513	0	0_0^0	$(1)^1A' \leftarrow \tilde{X}^1A'$
478.0		20919	406	406	
474.3		21083	570	570	
472.5		21165	652	652	
470.4		21260	747	747	
466.6		21432	919	919	
465.6		21478	965	570 + 406	
463.6		21568	1055	1055	
462.1		21639	1126	2 × 570	
459.5		21761	1248	570 + 652	
458.3		21819	1306	570 + 747	
456.1		21925	1412		
455.0		21979	1466		
453.9	**3.03**/*2.77*	22032	1519		$(2)^1A' \leftarrow \tilde{X}^1A'$
451.3		22157	1644	3 × 570	
447.8		22333	1820		
445.0		22470	1957		
439.9		22735	2222		
437.7		22848	2335		
428.3		23347	2834		
424.4		23560	3047		
378.6 (0.21)	**3.53**/*3.21*	26414	0	0_0^0	$(3)^1A' \leftarrow \tilde{X}^1A'$
279.2 (0.068)	**4.46**/*4.41*	35812	0	0_0^0	$(4)^1A' \leftarrow \tilde{X}^1A'$
274.7		36406	594	594	
1H-Py					
389.1	**3.85**	25702	0	0_0^0	$(4)^2A' \leftarrow \tilde{X}^2A'$
380.3		26293	591	591	
377.9		26464	762	762	
375.2		26653	951	951	
372.1		26871	1169	2 × 591 or 1169	
368.4		27147	1445	1445	
366.2		27310	1608	951 + 591 or 1608	
364.5		27435	1733	951 + 762	

[a] Relative integrated intensities of observed systems given in parentheses. [b] Bold, MP2/CC2/cc-pVDZ; italic, TD DFT/BLYP/TZVP. [c] Vibrational assignments based on the a′ modes in the electronic ground state of 1H-Py^+ and the corresponding neutral obtained with DFT/BLYP/cc-pVDZ: ν_{48} 445, ν_{44} 578, ν_{43} 667, ν_{41} 779, ν_{39} 925, and ν_{36} 1071 cm^1 for 1H-Py+; ν_{44} 574, ν_{41} 775, ν_{37} 968, ν_{30} 1181, ν_{17} 1452, and ν_{11} 1615 cm^1 for 1H-Py.

Experiments have also been carried out to detect fluorescence of H-Py^+ using the setup as already described.[29] Every distinct band seen in the absorption spectrum of H-Py^+ selectively excited with a tunable laser led to fluorescence. Identical, structured emission with origin at ~487 nm was detected irrespective of the laser wavelength in the 487−424-nm region, as well as upon excitation of the second (378 nm) and third (279 nm) absorption systems of H-Py^+. In all cases, rapid relaxation to the $v = 0$ level of the S_1 state takes place, followed

Scheme 1. Lowest-Energy Isomer of Protonated Pyrene

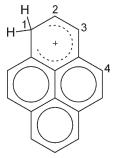

by the $S_1 \rightarrow S_0$ fluorescence. These observations confirm that the absorption band systems at 487, 378, and 279 nm belong to the same species, that is, to the same isomer of protonated pyrene.

Pyrene has three nonequivalent protonation sites located at carbon atoms 1, 2, and 4 (Scheme 1). To assign the observed absorptions of H-Py$^+$ to a specific isomer, theoretical calculations are needed. The ground-state energies of these isomers were computed with the ab initio RI-MP2 method[30] using the cc-pVDZ basis set.[31] Additionally, RI-DFT calculations[32] with the BLYP[33,34] functional and the TZVP basis set[35] were carried out on the H-Py$^+$ isomers. All calculations were done with the TURBOMOLE program package.[36]

The relative energies obtained with the two methods are similar (Table 2). The lowest-energy isomer is 1H-Py$^+$ (C_s symmetry, ^{1}A′ ground state). The other two, 4H-Py$^+$ and 2H-Py$^+$, are predicted to be 45 and 67 kJ/mol higher in energy, respectively, according to the calculations at the MP2 level. Thus, the excess energy of ∼120 kJ/mol, which is the difference of the PAs of the two reactants in the reaction of Py with H-Eth$^+$, is sufficient to give rise to any of these isomers.

Vertical excitation energies were determined for all three isomers with CC2/cc-pVDZ[37] and TD DFT/BLYP/TZVP; the results are compared in Table 2. The latter method gives the electronic transitions of the H-Py$^+$ isomers ∼0.3 eV higher in energy than the coupled-cluster approach, CC2. Small differences in the oscillator strengths are seen, but the general patterns are similar.

The electronic excitation energies of the three H-Py$^+$ isomers differ substantially. The three strongest transitions for the most stable isomer, 1H-Py$^+$, obtained by the CC2 method are predicted in the 2.8−3.5 eV range, close to the two systems observed at 487 and 378 nm (2.54 and 3.27 eV respectively). The other two isomers are predicted to absorb strongly in the UV range; furthermore, their first allowed transitions are at around 680−620 nm (1.8−2.0 eV). These are much lower in energy than the first transition assigned here to H-Py$^+$. Therefore and because this is the lowest-energy isomer, it is concluded that the observed absorption bands are due to 1H-Py$^+$.

The lowest-energy transition of 1H-Py$^+$ is predicted at 475 nm (2.61 eV) by TD DFT and at 443 nm (2.80 eV) by the CC2 method. Thus, the 487-nm absorption system is attributed to the $(1)^1A' \leftarrow \tilde{X}\ ^1A'$ transition of 1H-Py$^+$. The CC2 calculations overestimate its energy by 0.25 eV (Table 2). Taking such a shift into account, the observed system at 378 nm is assigned to the $(3)^1A' \leftarrow \tilde{X}\ ^1A'$ transition of this isomer. Both the CC2 and the TD DFT methods predict an additional absorption system of 1H-Py$^+$ around 440−450 nm (∼2.8 eV) due to the $(2)^1A' \leftarrow \tilde{X}\ ^1A'$ transition. As is seen from Figure 3, there is a congestion of vibrational bands of the $(1)^1A' \leftarrow \tilde{X}\ ^1A'$ system in this region. It is difficult to conclude from the present experimental data whether there is an additional electronic absorption band in this range. The highest-energy electronic transition observed at 279 nm is due to the $(4)^1A' \leftarrow \tilde{X}\ ^1A'$ excitation of

Table 2. Excited-State Symmetries, Vertical Excitation Energies and Oscillator Strengths for Protonated Pyrenes Obtained with TD DFT at the BLYP/TZVP Level of Theory and with the MP2/CC2 Method and the cc-pVDZ Basis Set[a]

TD DFT/BLYP/TZVP			MP2/CC2/cc-pVDZ		
exc. state	Δ*E* (eV)	*f*	exc. state	Δ*E* (eV)	*f*
		1H-Py$^+$, $\tilde{X}^1A'$, C_s			
	(0)			(0)	
$^1A'$	2.61	0.04	$^1A'$	2.8	0.18
$^1A'$	2.77	0.20	$^1A'$	3.03	0.21
$^1A'$	3.21	0.08	$^1A'$	3.53	0.16
$^1A'$	3.79	0.001	$^1A'$	4.46	0.02
$^1A'$	4.41	0.01	$^1A'$	5.12	0.03
$^1A'$	4.71	0.01	$^1A'$	5.18	0.02
		4H-Py$^+$, $\tilde{X}^1A'$, C_s			
	(43.3)			(44.8)	
$^1A'$	1.40	0.02	$^1A'$	1.87	0.05
$^1A'$	2.24	0.06	$^1A'$	2.53	0.11
$^1A'$	2.97	0.005	$^1A'$	3.62	0.002
$^1A'$	3.58	0.01	$^1A'$	4.22	0.01
			$^1A'$	4.44	0.07
			$^1A'$	4.61	0.19
		2H-Py$^+$, $\tilde{X}^1A_1$, C_{2v}			
	(57.2)			(66.8)	
$^1B_2$	1.8	0.04	$^1B_2$	2.02	0.07
$^1A_1$	2.81	0.004	$^1A_1$	3.19	0.04
$^1A_1$	2.82	0.001	$^1A_1$	3.48	0.0001
$^1B_2$	3.64	0.03	$^1B_2$	4.11	0.03
$^1A_1$	3.94	0.63	$^1A_1$	4.40	0.96
$^1B_2$	3.96	0.006	$^1B_2$	4.67	0.006
$^1B_2$	4.24	0.01	$^1B_2$	4.98	0.04
$^1B_2$	4.26	0.02	$^1A_1$	5.40	0.34
$^1A_1$	4.56	0.04			
$^1A_1$	4.83	0.12			

[a] Relative ground-state energies (kJ/mol) with respect to the most stable isomer given in parentheses.

the same isomer. Tentative assignment of the vibrational bands of the systems is based on the harmonic ground-state frequencies of 1H-Py$^+$ calculated with DFT/BLYP/cc-pVDZ, which are given in Table 1 as footnote [c].

The strong absorption at 389 nm is of the neutral 1H-Py radical. According to CC2 calculations, 1H-Py has three weak transitions in the 410−350 nm (3−3.5 eV) range (all with oscillator strengths of $f \sim 0.002$) followed by a strong band at around 330 nm (3.85 eV) with $f \sim 0.28$. This is not far from the observed band system. No other bands were detected in the experiment. 1H-Py has been detected using laser- and flash-photolysis of Py and dihydro-pyrene in amines solutions[38] and by VUV photolysis of Py in CO matrixes.[39] The spectra reported show three broad bands starting at around 400 nm. An oscillator strength of ∼0.09 for this transition has been derived;[39] it is about 3 times lower than that predicted by the present calculations. It was possible to estimate the *f* value of the strongest absorption of 1H-Py$^+$ at 487 nm by employing the reported value for the 1H-Py radical.[39] This was done by evaluating the

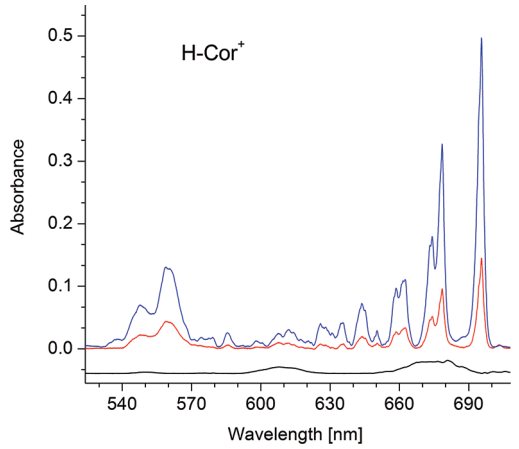

Figure 4. Long-wavelength part of the electronic absorption spectra recorded after deposition of $C_{24}H_{13}^+$ (blue) and after UV irradiation of the matrix (red). The bottom trace shows absorptions of coronene cation.

integrated intensity change of 1H-Py$^+$ and its neutral absorptions that resulted from UV irradiation. The value obtained is 0.13, if it is assumed that no process other than neutralization is involved. This is close to the 0.17 value predicted by the CC2 method.

3.2. Protonated Coronene. Deposition of m/z = 301 cations produced in the reaction of Cor with H-Eth$^+$ into a neon matrix resulted in two strong electronic systems in the visible range originating at 695 and 560 nm (Figure 4, blue trace). They are of cationic origin because they lose intensity after irradiation with UV photons (Figure 4, red line). In addition to these, known transitions of Cor$^+$ are seen throughout the measured region starting from ∼950 nm.[40] Its electronic spectrum was measured anew for a direct comparison. The Cor$^+$ absorptions are observed in the spectrum for the same reasons as in the case of H-Py$^+$ (section 3.1). Approximately, every fourth Cor molecule contains one ^{13}C atom and contributes to the intensity of the m/z = 301 peak in the mass spectrum. Fragmentation through H loss is the lowest dissociation channel for all smaller H-PAH$^+$s[11] except protonated benzene[10] (where the H_2 loss is dominant) and might also be true for Cor. Additionally, the mass resolution for H-Cor$^+$ was worse than for the lighter ions.

In the spectral range shown in Figure 4, Cor$^+$ has two broad, weak bands at 680 and 616 nm (Figure 4, black trace). The spectrum is scaled to match the intensity of the distinct bands in the range of 800−950 nm of Cor$^+$ that is present in the matrix together with H-Cor$^+$. The Cor$^+$ absorptions are too weak to contribute to the strong bands mentioned above. Therefore, the absorption systems of Figure 4 at 695 and 560 nm are from H-Cor$^+$. The first shows a long progression in the ∼360 and 457 cm^{-1} modes and their combination bands. Each of the bands has a higher-energy shoulder spaced from the sharper maximum by ∼24 cm^{-1}. The latter are zero-phonon bands followed by side bands, often observed in matrix spectra. The second system consists of three broad bands spaced by ∼ 370 cm^{-1}. Wavelengths of the observed bands are given in Table 3.

The short-wavelength part of the spectrum contains a number of overlapping systems of cationic and neutral species (Figure 5, green trace). It is dominated by a strong band at 470 nm, which is due to a neutral because it grows after UV irradiation. Cor$^+$ is also seen in this region; its absorption is hidden underneath the strong band of a neutral species. A part of the Cor$^+$ spectrum is

Table 3. Observed Band Maxima (±0.1 nm) and Their Assignments for Protonated Coronene and the Corresponding Neutral Coronenyl Radical[a] in a Neon Matrix, and the Calculated Vertical Excitation Energies ΔE

λ (nm)	ΔE^b (eV)	$\tilde{\nu}$ (cm^{-1})	$\Delta\tilde{\nu}$ (cm^{-1})	assignment[c]	
H-Cor$^+$					
695.6 (1)	**2.0**/*1.70*[d]	14377	0	0_0^0	$(1)^1A' \leftarrow \tilde{X}^1A'$
678.5		14738	361	361	
674.1		14834	457	457	
662.5		15095	718	2 × 361	
658.5		15186	809	457 + 361	
650.2		15379	1002	3 × 361	
645.2		15499	1122	457 + 2 × 361	
643.7		15534	1157		
638.4		15664	1287	4 × 361	
635.6		15732	1355	1355	
630.8		15854	1477	457 + 3 × 361	
628.1		15921	1544		
625.7		15981	1604		
614.3		16280	1903		
611.8		16344	1967		
607.5		16462	2085		
585.5		17078	2701	2 × 1355	
579.1		17268	2891		
574.2		17415	3038		
559.8 (0.56)	**2.41**/*2.11*	17865	0	0_0^0	$(2)^1A' \leftarrow \tilde{X}^1A'$
548.4		18235	370	370	
537.4		18607	742	2 × 370	
447.6 (0.22)	**3.03**/*2.62*	22341	0	0_0^0	$(3)^1A' \leftarrow \tilde{X}^1A'$
439.1		22773	432		
346.3 (0.29)	**3.79**/*3.14*	28876	0	0_0^0	$(5)^1A' \leftarrow \tilde{X}^1A'$
H-Cor					
776.5 (0.015)	**2.78**	12878	0	0_0^0	$(1)^2A' \leftarrow \tilde{X}^2A'$
755.6		13235	357		
479.3 (1)	**3.44**	20863w			
469.9		21279	0	0_0^0	$(3)^2A' \leftarrow \tilde{X}^2A'$
462.0		21646	367	367	
447.1		22367	1088		
441.3		22661	1382		
401.2 (0.37)	**3.72**	24928	0	0_0^0	$(5)^2A' \leftarrow \tilde{X}^2A'$

[a] Relative integrated intensities of observed systems given in parentheses. [b] Bold, MP2/CC2/def2-SVP; italic, TD DFT/BLYP/TZVP. [c] Vibrational assignments based on the a′ modes in the electronic ground state of protonated coronene and the corresponding neutral calculated with DFT/BLYP/TZVP; assignments are not unambiguous, because several modes have frequencies within ±30 cm^{-1} of the observed values. H-Cor$^+$: ν_{68-70} 369, 358, 355; ν_{63-66} 485, 483, 466, 462; ν_{27-30} 1389, 1379, 1374, 1352 cm^{-1}. H-Cor: ν_{67-70} 374, 368, 356, 353; ν_{47-48} 1130, 1122; ν_{26-28} 1408, 1399, 1378 cm^{-1}. [d] Previous calculations at the BLYP/6-31G* level yielded excitation energies of 1.74, 2.15, and 2.67 eV for the three lowest electronic transitions (ref 5).

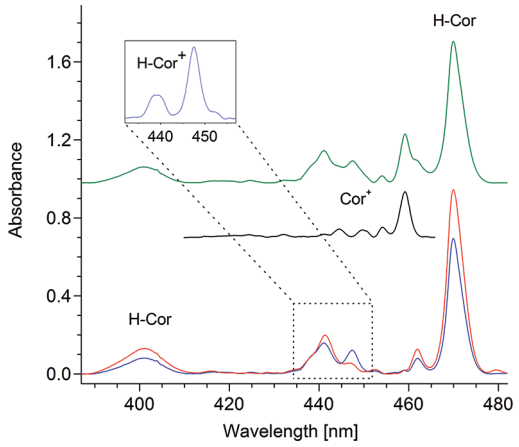

Figure 5. Short-wavelength part of the electronic absorption spectrum recorded after deposition of $C_{24}H_{13}^+$ cations into a neon matrix (green trace). Spectral features due to protonated coronene, the corresponding neutral radical, and coronene cation are present. The blue and red traces were observed upon deposition and after photobleaching, respectively, and after subtracting the absorption bands of coronene cation (black trace). The $(3)^1A' \leftarrow \tilde{X}^1A'$ transition of protonated coronene is shown in the inset, obtained after downscaling the red trace to the intensity of the absorption at 469 nm on the blue one and subtracting from it.

shown as the black trace in Figure 5, normalized to the same intensity as described. The blue trace was recorded after deposition of H-Cor$^+$ and subtraction of the bands of Cor$^+$, thus representing part of the "pure" spectrum of H-Cor$^+$ and the neutral H-Cor. The same procedure was applied for the spectrum recorded after UV irradiation of the matrix (Figure 5, red trace). The band centered at 447 nm is lower in intensity after photobleaching and, therefore, corresponds to the third transition of H-Cor$^+$. It is obscured by the strong absorption system originating at 470 nm and can be seen better after scaling and subtracting the spectrum recorded after deposition from that obtained after irradiation (inset of Figure 5). Additionally, a weak absorption of H-Cor$^+$ was detected in the UV range at 346 nm. It is not shown because of the presence of bands of neutral and cationic coronene in its vicinity.

The system at 470 nm and a broad system centered at 401 nm (Figure 5) are of neutral origin. In addition, a weak vibronic system at 776 nm was detected. These belong to H-Cor, which is formed by neutralization of H-Cor$^+$ by electrons released from Cl^- during UV irradiation of the matrix. The bands do not coincide with known absorptions of neutral Cor, which could also be formed under such conditions.

To support the assignment of the observed electronic transitions of H-Cor$^+$ and H-Cor, excitation energies were calculated using two approaches. All of the protonation sites of Cor are equivalent when only the periphery of the carbon skeleton is taken into account; therefore, only one isomer of H-Cor$^+$ and its neutral counterpart was considered. The geometry was optimized at the RI-MP2/def2-SVP and DFT/BLYP/TZVP levels of theory. CC2 with the def2-SVP basis set[41] and TD DFT at the BLYP/TZVP level were applied to calculate the excitation energies. The computational results are given in Table 3.

As can be seen, CC2 calculations overestimate the excitation energies for H-Cor$^+$ by around 0.2 eV, whereas the TD DFT method underestimates them by ~0.15 eV. The assignment of the observed transitions of H-Cor$^+$ in a neon matrix is based on theoretical predictions and is given in Table 3. Less accurate are the calculated intensities. The oscillator strength of the first electronic transition of H-Cor$^+$ is 0.11, whereas the second one is predicted to be stronger with $f \sim 0.18$ according to the CC2 calculations (Table 3). TD DFT gives the f values for these transitions as 0.04 and 0.1, respectively. Similar intensities for electronic transitions of H-Cor$^+$ were obtained when calculated with TD DFT using the same BLYP functional in conjunction with the 6-311G** basis set.[5] Hence, the results do not depend strongly on the method and basis set used. The strongest observed absorption system is assigned to the $(1)^1A' \leftarrow \tilde{X}^1A'$ transition observed at 695 nm, followed by the approximately half as strong transition at 560 nm.

Excitation energies of H-Cor were calculated using MP2/CC2/def2-SVP. Its strongest electronic transition $(3)^2A' \leftarrow \tilde{X}^2A'$ is predicted around 365 nm (3.4 eV; $f \sim 0.23$), 0.8 eV higher than the observed value . The lowest electronic excitation is calculated to occur at 443 nm (2.8 eV) and is 2 orders of magnitude less intense. Its energy is 1.2 eV higher than the band system observed at 776 nm, and the integrated intensity is about 50 times less than that of the 469-nm system. The calculated excitation energies for H-Cor show less good agreement with the observations than those for H-Cor$^+$. This is not surprising because of the open-shell electronic structure of H-Cor. The computational results are presented in Table 3, along with the assignment of the observed electronic bands. The vibrational assignment is based on the computed harmonic frequencies in the $^2A'$ ground state of H-Cor.

4. ASTRONOMICAL COMPARISON

One of the motivations for this study was to explore whether electronic transitions of protonated PAHs are relevant to the diffuse interstellar absorption bands (DIBs). First discussed as a possibility over 10 years ago,[3,4] this issue was studied recently through TD DFT calculations of electronic transitions of H-Cor$^+$ and protonated ovalene.[5] An interesting characteristic of H-PAH$^+$s is the existence of allowed electronic transitions in the visible part of the spectrum where most of the DIBs are found. Protonated PAHs are not unique in this respect, as large PAH neutrals, radicals, radical cations, and anions can also exhibit bands falling in the general region of DIBs. This has been illustrated in the experiments reported here and in other studies.[42] Nevertheless, H-PAH$^+$s are generally closed-shell molecules, which makes them good candidates from the perspective of interstellar chemistry.[3,4]

The present neon matrix data provide an improved basis for comparison with astronomical spectra, although one that still falls far short of the required laboratory gas-phase spectra. Based on the behavior of small systems[43] as well as a range of molecules similar to those studied here, it is anticipated that the wavenumbers for the gas-phase transitions of H-PAH$^+$ systems will lie within 200 cm^{-1} of the neon matrix values, whereas the band separations deduced from the vibrational structure should be about two orders of magnitude better.

In the case of H-Cor$^+$, there is a strong, narrow electronic transition at 695.6 nm with extended vibrational band structure and weaker, broader ones at 559.8 and 447.6 nm. For H-Cor$^+$ to be considered as a DIB candidate, there must be a reasonable correspondence in wavelength, overall spectral pattern, and relative band intensity between laboratory and astronomical

data. From the matrix measurements, it is expected that the origin band of the $(1)^1A' \leftarrow \tilde{X}\ ^1A'$ transition will fall in the 685−705-nm range. Examination of published diffuse band data for HD 183143 and HD 204827,[44,45] for example, shows that the most prominent narrow unidentified absorption within this range is the λ6993 DIB, which has an asymmetric profile.[46] Using the measured spectral intervals listed in Table 3, the strongest additional gas-phase bands of the $(1)^1A' \leftarrow \tilde{X}\ ^1A'$ system would then be expected in the ranges of 682.1, 677.7, 665.9, and 661.9 nm, where the first listed should have an intensity around two-thirds that of the origin band. We are not able to identify DIBs that satisfy these criteria; the situation is made particularly complicated because of the high number of narrow DIBs falling in the 670−690-nm range. Given the uncertainties in predicting gas-phase transition wavenumbers and the high DIB density in this region, the chances of an accidental "match" are high.

For H-Py$^+$, the origin band of the $(1)^1A' \leftarrow \tilde{X}\ ^1A'$ system falls at 487.5 nm in the neon matrix and, so, likely between 483 and 493 nm in the gas phase; only one DIB in HD 183143 falls within this range (λ4882 with a fwhm of ∼1.1 nm); a search for the next two bands in the series reveals no candidates. In HD 204827, weaker, narrower DIB candidates fall within the wavelength range of interest but do not have plausible features at higher frequency.

AUTHOR INFORMATION

Corresponding Author

*E-mail: j.p.maier@unibas.ch. Tel.: +41 61 267 38 26. Fax: +41 61 267 38 55.

ACKNOWLEDGMENT

This work was supported financially by the Swiss National Science Foundation (Project 200020-124349/1).

REFERENCES

(1) Tielens, A. G. G. M. *Annu. Rev. Astron. Astrophys.* **2008**, *46*, 289 and references therein.
(2) Hudgins, D. M.; Bauschlicher, C. W.; Allamandola, L. J. *Spectrochim. Acta, Part A* **2001**, *57*, 907.
(3) LePage, V.; Keheyan, Y.; Bierbaum, V. M.; Snow, T. P. *J. Am. Chem. Soc.* **1997**, *119*, 8373.
(4) Snow, T. P.; Le Page, V.; Keheyan, Y.; Bierbaum, V. M. *Nature* **1998**, *391*, 259.
(5) Pathak, A.; Sarre, P. J. *Mon. Not. R. Astron. Soc.* **2008**, *391*, L10.
(6) Ricks, A. M.; Douberly, G. E.; Duncan, M. A. *Astrophys. J.* **2009**, *702*, 301.
(7) Solca, N.; Dopfer, O. *Angew. Chem., Int. Ed.* **2002**, *41*, 3628.
(8) Lorenz, U. J.; Solca, N.; Lemaire, J.; Maitre, P.; Dopfer, O. *Angew. Chem., Int. Ed.* **2007**, *46*, 6714.
(9) Douberly, G. E.; Ricks, A. M.; Schleyer, P. V. R.; Duncan, M. A. *J. Phys. Chem. A* **2008**, *112*, 4869.
(10) Jones, W.; Boissel, P.; Chiavarino, B.; Crestoni, M. E.; Fornarini, S.; Lemaire, J.; Maitre, P. *Angew. Chem., Int. Ed.* **2003**, *42*, 2057.
(11) Knorke, H.; Langer, J.; Oomens, J.; Dopfer, O. *Astrophys. J. Lett.* **2009**, *706*, L66.
(12) Olah, G. A.; Pittman, C. U.; Waack, R.; Doran, M. *J. Am. Chem. Soc.* **1966**, *88*, 1488.
(13) Stuart, A. A. V.; Mackor, E. L. *J. Chem. Phys.* **1957**, *27*, 826.
(14) Dallinga, G.; Mackor, E. L.; Stuart, A. A. V. *Mol. Phys.* **1958**, *1*, 123.
(15) Reid, C. *J. Am. Chem. Soc.* **1954**, *76*, 3264.
(16) Perkampus, H.; Baumgarten, E. *Angew. Chem., Int. Ed.* **1964**, *3*, 776.
(17) Garkusha, I.; Fulara, J.; Nagy, A.; Maier, J. P. *J. Am. Chem. Soc.* **2010**, *132*, 14979.
(18) Garkusha, I.; Fulara, J.; Nagy, A.; Maier, J. P. *Astrophys. J.* **2011**, *728*, 131.
(19) Alata, I.; Omidyan, R.; Broquier, M.; Dedonder, C.; Dopfer, O.; Jouvet, C. *Phys. Chem. Chem. Phys.* **2010**, *12*, 14456.
(20) Alata, I.; Dedonder, C.; Broquier, M.; Marceca, E.; Jouvet, C. *J. Am. Chem. Soc.* **2010**, *132*, 17483.
(21) Fulara, J.; Nagy, A.; Garkusha, I.; Maier, J. P. *J. Chem. Phys.* **2010**, 133, 024304.
(22) Munson, M. S. B.; Field, F. H. *J. Am. Chem. Soc.* **1966**, *88*, 2621.
(23) Hunter, E. P. L.; Lias, S. G. *J. Phys. Chem. Ref. Data* **1998**, *27*, 244.
(24) Lorenz, U. J.; Lemaire, J.; Maitre, P.; Crestoni, M.-E.; Fornarini, S.; Dopfer, O. *Int. J. Mass Spectrom.* **2007**, *267*, 43.
(25) Mass Spectra. In *NIST Chemistry WebBook*; NIST Standard Reference Database Number 69; Linstrom, P. J., Mallard, W. G., Eds.; National Institute of Standards and Technology: Gaithersburg, MD, 2005; available at http://webbook.nist.gov/chemistryAccessed June 2011.
(26) Salama, F.; Allamandola, L. J. *J. Chem. Soc., Faraday Trans.* **1993**, *89*, 2277.
(27) Vala, M.; Szczepanski, J.; Pauzat, F.; Parisel, O.; Talbi, D.; Ellinger, Y. *J. Phys. Chem.* **1994**, *98*, 9187.
(28) Liu, X. S.; Iu, K. K.; Thomas, J. K.; He, H. Y.; Klinowski, J. *J. Am. Chem. Soc.* **1994**, *116*, 11811.
(29) Nagy, A.; Fulara, J.; Maier, J. P. *J. Am. Chem. Soc.* **2011** manuscript submitted.
(30) Weigend, F.; Häser, M. *Theor. Chem. Acc.* **1997**, *97*, 331.
(31) Woon, D. E.; Dunning, J. T. H. *J. Chem. Phys.* **1993**, *98*, 1358.
(32) Sierka, M.; Hogekamp, A.; Ahlrichs, R. *J. Chem. Phys.* **2003**, *118*, 9136.
(33) Becke, A. D. *Phys. Rev. A* **1988**, *38*, 3098.
(34) Lee, C.; Yang, W.; Parr, R. G. *Phys. Rev. B* **1988**, *37*, 785.
(35) Schäfer, A.; Huber, C.; Ahlrichs, R. *J. Chem. Phys.* **1994**, *100*, 5829.
(36) Ahlrichs, R.; Bär, M.; Häser, M.; Horn, H.; Kölmel, C. *Chem. Phys. Lett.* **1989**, *162*, 165.
(37) Hattig, C.; Kohn, A. *J. Chem. Phys.* **2002**, *117*, 6939.
(38) Okada, T.; Mori, T.; Mataga, N. *Bull. Chem. Soc. Jpn.* **1976**, *49*, 3398.
(39) Bouwman, J.; Cuppen, H. M.; Bakker, A.; Allamandola, L. J.; Linnartz, H. *Astron. Astrophys.* **2010**, *511*, A33.
(40) Ehrenfreund, P.; D'Hendecourt, L.; Verstraete, L.; Leger, A.; Schmidt, W.; Defourneau, D. *Astron. Astrophys.* **1992**, *259*, 257.
(41) Schäfer, A.; Horn, H.; Ahlrichs, R. *J. Chem. Phys.* **1992**, *97*, 2571.
(42) Hammonds, M.; Pathak, A.; Candian, A.; Sarre, P. J. *EAS Publ. Ser.* **2011**, *46*, 373.
(43) Jacox, M. E. *J. Mol. Struct.* **1987**, *157*, 43.
(44) Hobbs, L. M.; York, D. G.; Thorburn, J. A.; Snow, T. P.; Bishof, M.; Friedman, S. D.; McCall, B. J.; Oka, T.; Rachford, B.; Sonnentrucker, P.; Welty, D. E. *Astrophys. J.* **2009**, *705*, 32.
(45) Hobbs, L. M.; York, D. G.; Snow, T. P.; Oka, T.; Thorburn, J. A.; Bishof, M.; Friedman, S. D.; McCall, B. J.; Rachford, B.; Sonnentrucker, P.; Welty, D. E. *Astrophys. J.* **2008**, *680*, 1256.
(46) Herbig, G. H.; Soderblom, D. R. *Astrophys. J.* **1982**, *252*, 610.